Editors' Suggestion Featured in Physics

Observation of Quantum Phase Synchronization in Spin-1 Atoms

Arif Warsi Laskar,[1] Pratik Adhikary,[1] Suprodip Mondal,[1] Parag Katiyar,[1] Sai Vinjanampathy,[2,3] and Saikat Ghosh[1,*]

[1]*Department of Physics, Indian Institute of Technology-Kanpur, Uttar Pradesh 208016, India*

[2]*Department of Physics, Indian Institute of Technology-Bombay, Powai, Mumbai 400076, India*

[3]*Centre for Quantum Technologies, National University of Singapore, 3 Science Drive 2, 117543 Singapore, Singapore*

(Received 14 November 2019; revised 10 April 2020; accepted 29 May 2020; published 1 July 2020)

With growing interest in quantum technologies, possibilities of synchronizing quantum systems have garnered significant recent attention. In experiments with dilute ensemble of laser cooled spin-1 ^{87}Rb atoms, we observe phase difference of spin coherences to synchronize with phases of external classical fields. An initial limit-cycle state of a spin-1 atom localizes in phase space due to dark-state polaritons generated by classical two-photon tone fields. In particular, when the two couplings fields are out of phase, the limit-cycle state synchronizes only with two artificially engineered, anisotropic decay rates. Furthermore, we observe a blockade of synchronization due to quantum interference and emergence of Arnold-tongue-like features. Such anisotropic decay induced synchronization of spin-1 systems with no classical analog can provide insights in open quantum systems and find applications in synchronized quantum networks.

DOI: 10.1103/PhysRevLett.125.013601

Spontaneous synchronization is abundant in nature, ranging from synchronized fireflies to neuronal activities [1,2]. Such synchronous dynamics, being stable to external perturbations, have also found a range of applications including satellites [3], electrical grids [4], clocks [5], and wind turbines [6]. Recently, synchronization in quantum domain has emerged as a field for understanding correlations [7–19] and for applications in quantum networks [7,20,21]. Early proposals focused on open quantum systems whose mean-field theories exhibited synchronization [10,21–23]. Such models were extended deep in the quantum regime and compared to finite dimensional systems that have no classical analogs [12,16,24]. In these systems, suitably chosen angles in phase space were found to be entrained to the phase of an external signal. Despite such proposals, observation of synchronization deep in the quantum regime has remained elusive.

Recently, it was pointed out that spin-1 is the smallest quantum system with a limit cycle in phase space that can synchronize to external tone phases [16,18]. Furthermore, Roulet *et al.* predicted that weak classical tones [represented as two coherent couplings $\eta_{-1,0}$, $\eta_{0,1}$, Fig. 1(a)] and anisotropic internal decay rates γ_g and γ_d can localize and synchronize the limit-cycle state, for all tone phases.

Here we report first observation of quantum synchronization with spin-1 systems, realized in a dilute ensemble of approximately a million laser-cooled ^{87}Rb atoms in $|F=1\rangle$ hyperfine ground-state manifold. Atoms are initialized to a limit-cycle in phase space, corresponding to the state $|F=1, m_F=0\rangle$ [Figs. 1(a) and 1(b)]. Synchronization is initiated with two circularly polarized *control* fields ($\Omega^{\pm}_{c(S)}$) along with a π-polarized *probe* Ω^{π}_{p}. These fields induce coherent two-photon couplings between the spin states $|F=1, m_F=\pm 1\rangle$ and $|F=1, m_F=0\rangle$ [Fig. 1(a), inset(i)] [25], corresponding to the weak tones $\eta_{-1,0}$, $\eta_{0,1}$ [16,18]. When the control fields are adiabatically switched off, the probe gets stored as two dark state polaritons (DSPs) in atomic coherences $\rho_{-1,0}$ and $\rho_{0,1}$ [26–32]. In the dark, the DSPs evolve in time, acquiring relative dynamic phase. From the retrieved DSPs as optical fields, we estimate the coherences and reconstruct a measure of synchronization. In particular, we observe a nonzero synchronization, for all tone phases, only when the two decay rates γ_g and γ_d are anisotropic [Fig. 1(a), inset(ii)]. We further observe a synchronization blockade due to destructive interference and emergence of Arnold-tongue-like features with increasing drive: these have been predicted as quintessential signatures of quantum synchronization [16,18].

Figures 1(d) and 1(e) show typical experimental time traces for probe pulses, with progressively increasing time of storage, with and without applied magnetic field, respectively. After cooling in a magneto-optic trap, the atoms are optically pumped in the ground state $|F=1, m_F=0\rangle$. A linearly polarized control, comprising two circularly polarized fields, is adiabatically switched on [at time instance t_I in Fig. 1(c)] and off (time t_{II}), after 1.6 μs, such that a probe pulse gets partially stored [see Supplemental Material [33]: S.V.(a)]. The corresponding coherences evolve and interfere in the dark due to an applied magnetic field (interval t_{III}, see the Supplemental Material [33]: S.III.). We observe oscillations in the retrieved pulse as the storage time ($\tau = t_{\mathrm{IV}} - t_{\mathrm{II}}$) is varied [Fig. 1(e)].

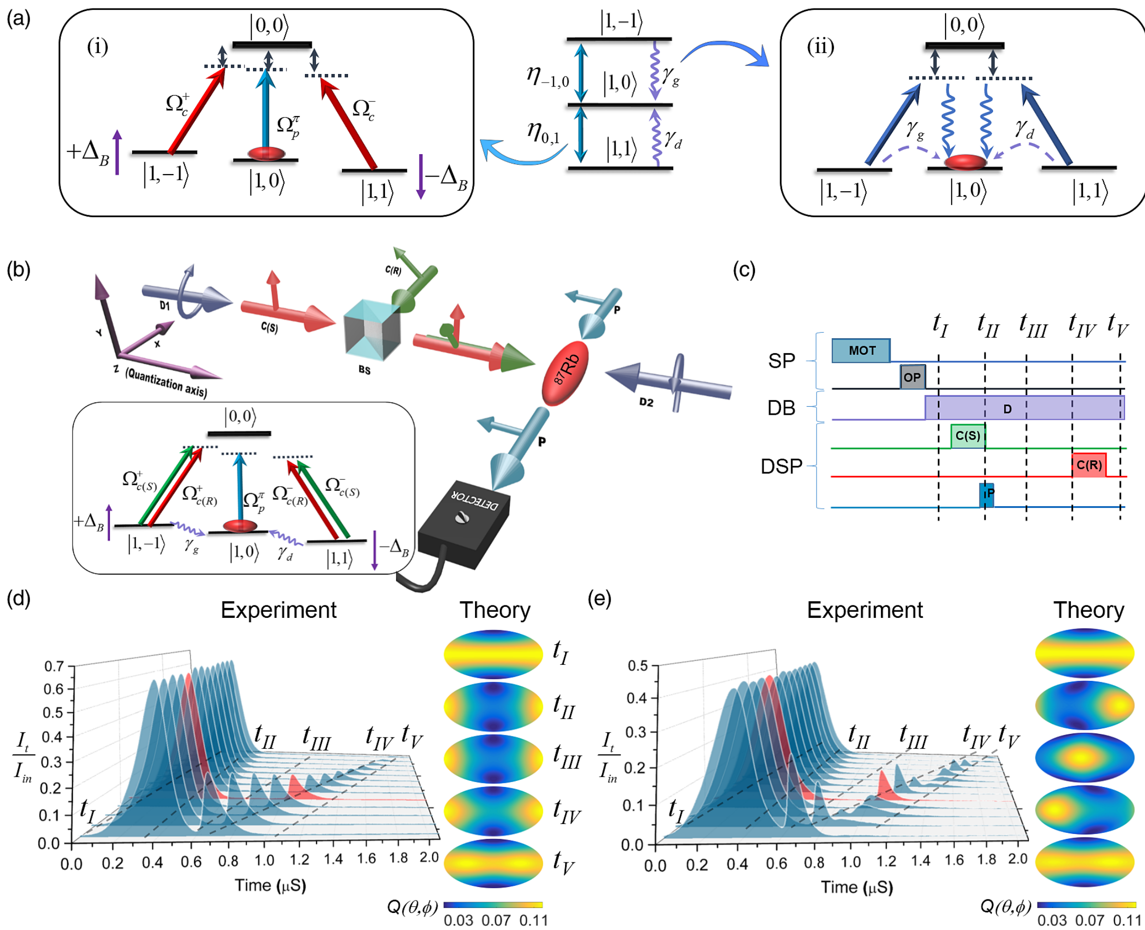

FIG. 1. (a) Energy level diagram of a spin-1 atom with coherent couplings $\eta_{-1,0}$ and $\eta_{0,1}$ along with *incoherent* decay rates γ_g and γ_d. (a.i) Coherent couplings are engineered using control ($\Omega_c^{\pm}$) and probe fields (Ω_p^{π}). Here Δ_B is the ground state energy shift due to a magnetic field along the quantization axis. (a.ii) Decay rates γ_g and γ_d are engineered with two fields coupling states $|1,-1\rangle$ and $|1,1\rangle$ to the excited state $|0,0\rangle$. (b) Experimental setup, showing propagation directions of storing [C(S), green] and retrieving [C(R), red] control fields, probe field (P, blue), and decay beams (D1 and D2, in violet, at small angles to control fields). Here BS: beam splitter. (c) Experimental timing sequence with intervals for state preparation (SP), decay beams (DB), and control-probe (DSP) fields. Here MOT: magneto optical trap; OP: optical pumping; D: decay beams. (d) Typical probe field time traces with varying storage times and with $\phi_c = \phi_d = 0$. Reconstructed Husimi-Q function from numerical simulations (corresponding to red time trace) are plotted at different times (with the horizontal and vertical axes corresponding to ϕ and θ, respectively, and $0 \leq \theta \leq \pi$ and $-\pi \leq \phi \leq \pi$). (e) In presence of magnetic field (with dynamic phase $\phi_d/\pi = 3.22$, and tone phase $\phi_c = 0$), the retrieved intensity oscillates with changing storage time. Corresponding Husimi-Q function gets localized and entrained with the dynamic phase, precessing in equatorial plane. Here $I_{\rm in}$ and I_t are input and transmitted probe intensities, respectively.

Numerically simulated time traces, in close agreement with observations (see the Supplemental Material [33]: S.IV.), are used to reconstruct the underlying spin-1 atomic state (corresponding to $|F=1\rangle$ manifold). In particular, a state $\hat{\rho}$ is visualized using Husimi-Q function, defined as [43–45]

$$Q(\theta,\phi) = \frac{3}{4\pi}\langle\theta,\phi|\hat{\rho}|\theta,\phi\rangle.$$

Here $|\theta,\phi\rangle = \cos^2(\theta/2)[|-1\rangle + \sqrt{2}e^{i\phi}\tan(\theta/2)|0\rangle + e^{i2\phi}\tan^2(\theta/2)|1\rangle]$ is a spin coherent state [46], parametrized by the angles θ and ϕ.

From Husimi-Q functions, plotted using Hammer projection [shown in red, Figs. 1(d) and 1(e)], we note that the initial state $|F=1, m_F=0\rangle$ corresponds to a limit-cycle (see the Supplemental Material [33]: S.II.) [16,18]. Between time instances $t_{\rm II}$ and $t_{\rm IV}$, the two in-phase ($\phi_c = 0$) control and the probe fields result in a localized state in phase space [Figs. 1(d) and 1(e) "Theory" plots in right panels]. In particular, with a magnetic field (B_z) along the quantization axis [Fig. 1(b)], the state gets entrained and precesses in the equatorial plane, resulting in an accumulated dynamic phase $\phi_d = 2\Delta_B\tau$ over a total storage time τ [Fig. 1(e)]. Here $\Delta_B = \mu_B B_z/2\hbar$ is the ground state shifts due to B_z [Fig. 1(a)] and μ_B is the Bohr magneton.

Figure 2(a) [2(c)] shows typical experimental (simulation) plots of the retrieved intensity, $I_R(\tau)$ at $\tau = 600$ ns, with changing tone (ϕ_c) and the dynamic phase (ϕ_d) (see the Supplemental Material [33]: S.III.). Tone phase is varied by changing the phase difference between the stored and retrieving control fields, and dynamic phase is scanned with a magnetic field [Fig. 1(b)]. In particular, at regions **A** (corresponding to $\phi_c = 0$) and **B** ($\phi_c = \pi$), the states in phase space appear dramatically different [Fig. 2(c)]. While the state gets localized at **A**, it remains a delocalized limit-cycle at **B** [Fig. 2(e), **A** and **B**, respectively]. However, when the artificially engineered decay rates [see the Supplemental Material [33]: S.V.(d)] are made anisotropic [$\gamma_d/\gamma_g = 11.00$, Figs. 2(b) and 2(d) for experiment and simulations, respectively], the state localizes for all tone phases including $\phi_c = 0$ and $\phi_c = \pi$ [Fig. 2(e), **C** and **D**, respectively].

These localized states can be quantified with a synchronization function, defined as [16,18] (see the Supplemental Material [33]: S.II.):

$$S(\phi) = \int_0^\pi Q(\theta,\phi)\sin\theta d\theta - \frac{1}{2\pi},$$
$$\simeq \frac{3}{8\sqrt{2}}[|\rho_{-1,0}|\cos(\Delta_B\tau+\phi) + |\rho_{0,1}|\cos(\Delta_B\tau+\phi+\phi_c)]$$

(with squeezing tone, $\rho_{-1,1} \simeq 0$). For a limit cycle state, $S(\phi)$ remains identically zero. Any nonzero $S(\phi)$ indicate localized, synchronized states in phase space. From the visibility of the interference fringes with ϕ_c [Figs. 2(a)–2(d)], we estimate the coherences $|\rho_{0,1}|$, $|\rho_{-1,0}|$ and their relative phases, thereby reconstructing the measure from experimental data [Figs. 2(f) and 2(g)] data and compare it with simulations [Figs. 2(h) and 2(i); see the Supplemental Material [33]: S.II.). Our estimated synchronization function $\tilde{S}(\phi)$, is related to the measure as $S(\phi) = \kappa\tilde{S}(\phi)$, where κ depends on normalization, retrieved field strength and optical depth.

We observe maximum of $\tilde{S}(\phi)$, i.e., $\tilde{S}_{\max}(\phi)$ to remain nonzero when the two tones are in phase [$\phi_c = 0$, Figs. 2(f) and 2(h)]. On the contrary, when the two tones are out of phase ($\phi_c = \pi$), $\tilde{S}_{\max}(\phi)$ sharply falls to zero. However, for anisotropic decay rates [Figs. 2(g) and 2(i)], $\tilde{S}_{\max}(\phi)$ is nonzero for all ϕ_c.

For out-of-phase tones, there is a rich interplay between incoherent and coherent dynamics [25,47]. When both decay rates are smaller than Δ_B, the coherences destructively interfere and the state remains a limit cycle. However, as the decay rates become comparable to Δ_B, the coherences interfere only partially, resulting in a localized state.

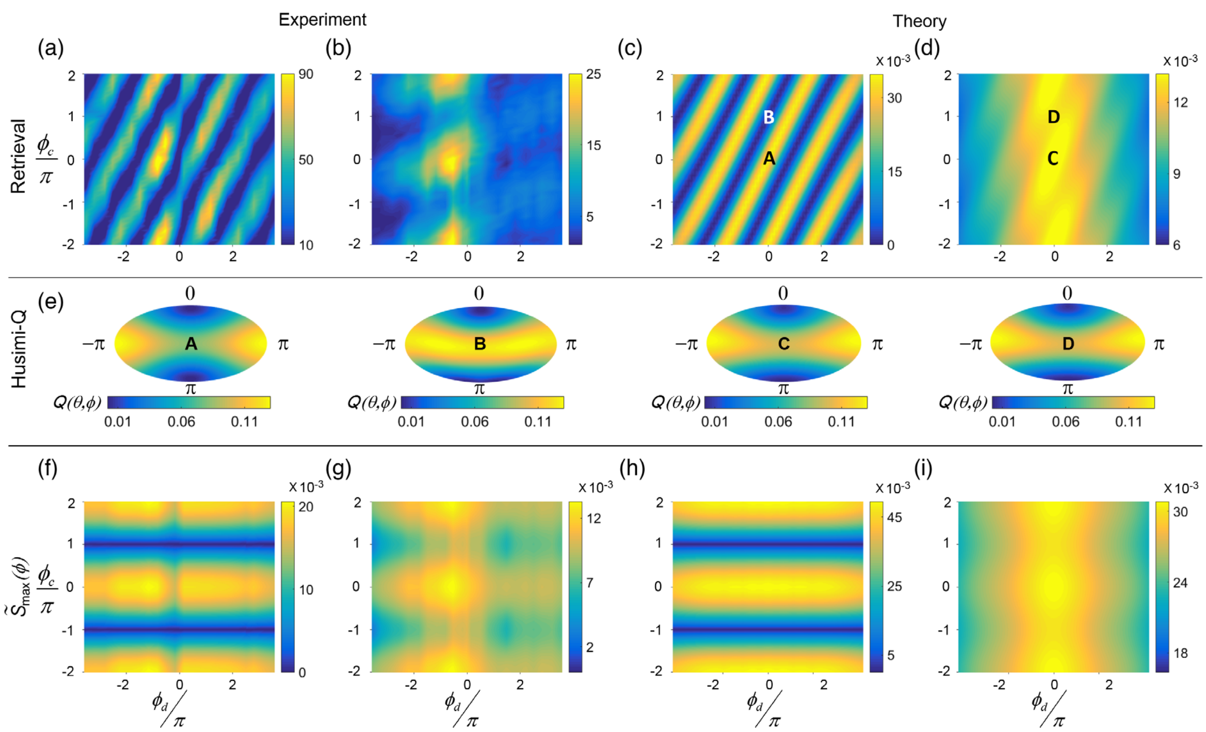

FIG. 2. (a), (b) Plots of retrieved intensity with dynamic (ϕ_d) and tone (ϕ_c) phases and with decay rate ratios: $\gamma_d/\gamma_g = 1.00$ (a) and 11.90 (b). ϕ_d is varied with magnetic field while keeping the storage time ($\tau = 600$ ns) fixed. (c), (d) Numerically simulated retrieved intensity for decay rate ratios: $\gamma_d/\gamma_g = 1.00$ (c) and 11.00 (d). (e) Husimi-Q plots for the regions A, B, C, and D of (c) and (d). (f)–(i) Maximum of synchronization function [$\tilde{S}_{\max}(\phi)$] calculated from experimental and simulated plots corresponding to (a),(b),(c), and (d). Here experimental parameters Ω_p^π, $\Omega_{c(S)}^{\rm lin}$, $\Omega_{c(R)}^{\rm lin}$, and γ_g are set to 0.64γ, 1.02γ, 1.44γ, and 107 kHz, respectively, and the simulation parameters are as tabulated in the Supplemental Material [33]. Color bars for experimental plots are in units of μW/cm^2 and for theory plots, in units of $2|\Omega_R|^2/\gamma^2$, where $|\Omega_R|$ and γ correspond to retrieved field and excited state decay, respectively.

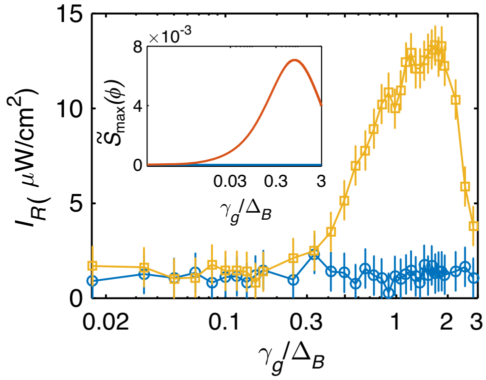

FIG. 3. Retrieved intensity at a region of destructive interference is plotted as a function of increasing γ_g, for a fixed Δ_B. Blue and yellow are for $\gamma_d/\gamma_g = 1.00$ and 11.90, respectively. Inset shows $\tilde{S}_{\max}(\phi)$, as extracted from experimental data. Blue and red correspond to Figs. 2(a) and 2(b), respectively. Here the experimental parameters Ω_p^π, $\Omega_{c(S)}^{\text{lin}}$, and $\Omega_{c(R)}^{\text{lin}}$ are set as in Fig. 2 with $\phi_c = 140°$ and $\Delta_B = 67$ kHz.

In Fig. 3, over an extended region ($\gamma_g < \Delta_B$), destructive interference (with $\phi_c = 140°$) causes a blockade of synchronization. Moreover, as the decay rates are made anisotropic ($\gamma_d > \gamma_g$), the estimated $\tilde{S}_{\max}(\phi)$ at a fixed ϕ_c becomes nonzero along with a finite retrieval. When both decay rates are large (γ_d, $\gamma_g > \Delta_B$), there is overall decrease in retrieval due to decoherence. Such *blockade* of synchronization due to quantum interference and re-emergence of entrained states are typical quantum signatures [14,18].

The state synchronizes over a range of dynamic phase (ϕ_d) and field strengths. Such dependence, leading to Arnold-tongue-like features, have been studied as typical signatures in classical and quantum synchronization [1]. Here, for out-of-phase tone and with increasing probe field (Ω_p^π) we observe fringes with varying magnetic field [Figs. 4(a) and 4(c)]. For equal decays, the states remain delocalized [typical regions **A**, **B**, and **C**, Figs. 4(c) and 4(e)] with $\tilde{S}_{\max}(\phi) \sim 0$ for all dynamic phases [estimated from simulations, Figs. 4(c), inset]. Furthermore, for anisotropic rates [$\gamma_d/\gamma_g = 11.00$, Figs. 4(b) and 4(d)], the fringes merge to a single maxima, broadening into a Arnold-tongue-like shape with increasing Ω_p^π. Since ϕ_c is kept constant, $\tilde{S}_{\max}(\phi)$ could not be evaluated from fringe visibility with tone phase. Nevertheless, when evaluated numerically, Arnold-tongue for $\tilde{S}_{\max}(\phi)$ emerges from a null background [Fig. 4(d), inset] along with localized states, entrained with ϕ_d [**D**, **E**, and **F**, Figs. 4(d) and 4(e)].

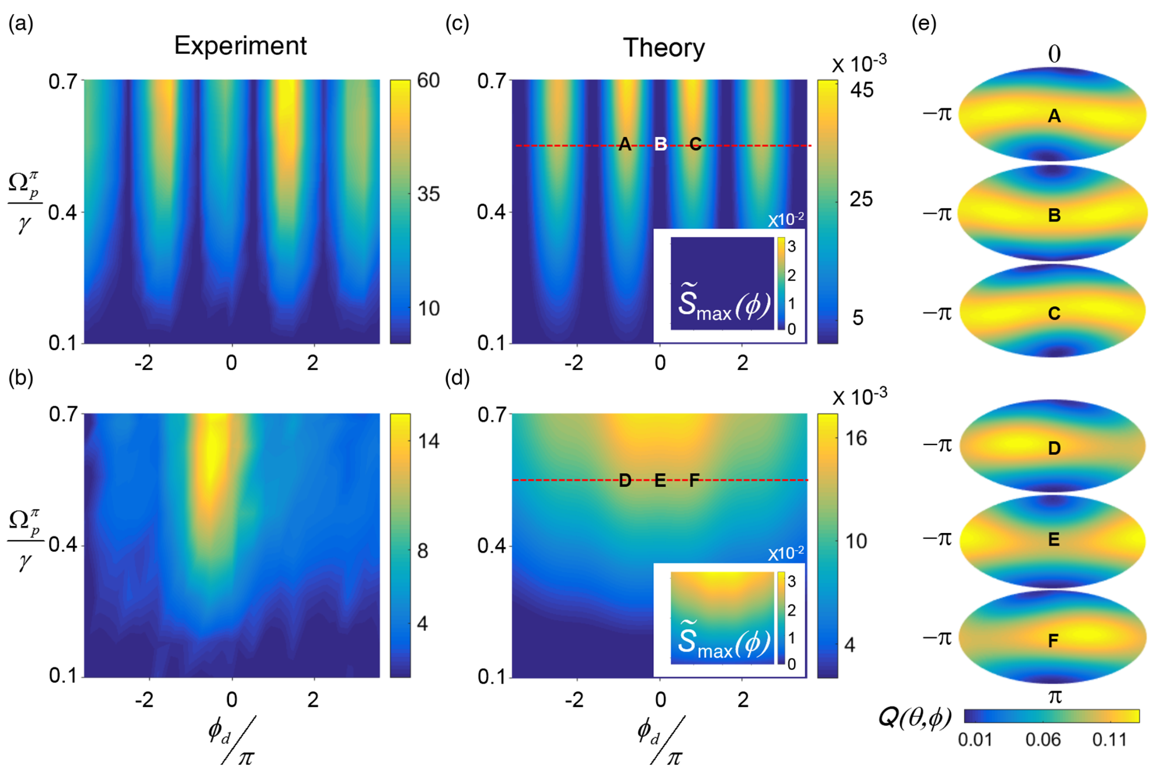

FIG. 4. (a),(b) Retrieved intensity, plotted with increasing probe field strength (Ω_p^π) and dynamic phase (ϕ_d) (storage time $\tau = 600$ ns), with $\gamma_d/\gamma_g = 1.00$ and 11.90 for (a) and (b), respectively. (c),(d) Simulated plots for $\gamma_d/\gamma_g = 1.00$ (c), and 11.00 (d). Insets of (c) and (d) are the corresponding $\tilde{S}_{\max}(\phi)$. (e) Husimi-Q plots for regions A, B, C and D, E, F of (c) and (d), respectively. Here experimental parameters $\Omega_{c(S)}^{\text{lin}}$, $\Omega_{c(R)}^{\text{lin}}$, and γ_g are set as in Fig. 2 and ϕ_c is set to 140°. Simulation parameters are as tabulated in the Supplemental Material [33]. Color bars for all the plots are as in Fig. 2.

To conclude, here we report first observation of synchronization in the smallest quantum system. Synchronization is achieved using two primary resources: quantum coherence and engineered decay rates. In particular, for anisotropic decay rates, limit-cycle states synchronize for all tone phases. Furthermore, we observe two typical quantum signatures: a synchronization blockade due to quantum interference and emergence of Arnold tongue in $\tilde{S}_{\max}(\phi)$. The experimentally observed Arnold tongue is narrower, which can bear signatures of superradiance [48]. A search for synchronization in multiple such spin systems, towards synchronized quantum memories can lead to applications in quantum networks.

We thank Sagar Chakraborty, Sourin Das, Anurag Gupta, M. Hajdušek, Umakant Rapol, and Harshawardhan Wanare for insightful discussions and comments. S. V., P. A., and S. M. acknowledge support from DST-SERB Early Career Research Award (ECR/2018/000957), UGC, and CSIR, respectively. This work was supported under SERB-DST Grant No. SERB/PHY/2015404.

*gsaikat@iitk.ac.in

[1] A. Pikovskij, M. Rosenblum, and K. Jurgen, *Synchronization: A Universal Concept in Nonlinear Sciences* (Cambridge University Press, Cambridge, England, 2007).
[2] S. Strogatz, *Sync: The Emerging Science of Spontaneous Order* (Penguin Books, UK, London, 2008).
[3] W. Lewandowski and E. F. Arias, Metrologia **48**, S219 (2011).
[4] M. Rohden, A. Sorge, M. Timme, and D. Witthaut, Phys. Rev. Lett. **109**, 064101 (2012).
[5] J.-D. Deschênes, L. C. Sinclair, F. R. Giorgetta, W. C. Swann, E. Baumann, H. Bergeron, M. Cermak, I. Coddington, and N. R. Newbury, Phys. Rev. X **6**, 021016 (2016).
[6] J. Cidras, A. E. Feijoo, and C. C. Gonzalez, IEEE Trans. Power Syst. **17**, 1162 (2002).
[7] H. J. Kimble, Nature (London) **453**, 1023 (2008).
[8] G. Manzano, F. Galve, G. L. Giorgi, E. Hernández-García, and R. Zambrini, Sci. Rep. **3**, 1439 (2013).
[9] A. Mari, A. Farace, N. Didier, V. Giovannetti, and R. Fazio, Phys. Rev. Lett. **111**, 103605 (2013).
[10] S. Walter, A. Nunnenkamp, and C. Bruder, Phys. Rev. Lett. **112**, 094102 (2014).
[11] T. E. Lee, C.-K. Chan, and S. Wang, Phys. Rev. E **89**, 022913 (2014).
[12] N. Lörch, E. Amitai, A. Nunnenkamp, and C. Bruder, Phys. Rev. Lett. **117**, 073601 (2016).
[13] T. Weiss, S. Walter, and F. Marquardt, Phys. Rev. A **95**, 041802(R) (2017).
[14] N. Lörch, S. E. Nigg, A. Nunnenkamp, R. P. Tiwari, and C. Bruder, Phys. Rev. Lett. **118**, 243602 (2017).
[15] T. Weiß, Nonlinear dynamics in quantum synchronization and topological transport, Ph.D. thesis, Naturwissenschaftliche Fakultät, 2017.
[16] A. Roulet and C. Bruder, Phys. Rev. Lett. **121**, 053601 (2018).
[17] S. Sonar, M. Hajdušek, M. Mukherjee, R. Fazio, V. Vedral, S. Vinjanampathy, and L.-C. Kwek, Phys. Rev. Lett. **120**, 163601 (2018).
[18] M. Koppenhöfer and A. Roulet, Phys. Rev. A **99**, 043804 (2019).
[19] A. Roulet and C. Bruder, Phys. Rev. Lett. **121**, 063601 (2018).
[20] L.-M. Duan, M. D. Lukin, J. I. Cirac, and P. Zoller, Nature (London) **414**, 413 (2001).
[21] T. E. Lee and H. R. Sadeghpour, Phys. Rev. Lett. **111**, 234101 (2013).
[22] D. Witthaut, S. Wimberger, R. Burioni, and M. Timme, Nat. Commun. **8**, 14829 (2017).
[23] V. M. Bastidas, I. Omelchenko, A. Zakharova, E. Schöll, and T. Brandes, Phys. Rev. E **92**, 062924 (2015).
[24] A. Cabot, G. L. Giorgi, F. Galve, and R. Zambrini, Phys. Rev. Lett. **123**, 023604 (2019).
[25] A. W. Laskar, N. Singh, P. Adhikary, A. Mukherjee, and S. Ghosh, Optica **5**, 1462 (2018).
[26] M. D. Lukin, S. F. Yelin, and M. Fleischhauer, Phys. Rev. Lett. **84**, 4232 (2000).
[27] C. Liu, Z. Dutton, C. H. Behroozi, and L. V. Hau, Nature (London) **409**, 490 (2001).
[28] D. F. Phillips, A. Fleischhauer, A. Mair, R. L. Walsworth, and M. D. Lukin, Phys. Rev. Lett. **86**, 783 (2001).
[29] M. Fleischhauer and M. D. Lukin, Phys. Rev. A **65**, 022314 (2002).
[30] L. Karpa, F. Vewinger, and M. Weitz, Phys. Rev. Lett. **101**, 170406 (2008).
[31] H. Wang, S. Li, Z. Xu, X. Zhao, L. Zhang, J. Li, Y. Wu, C. Xie, K. Peng, and M. Xiao, Phys. Rev. A **83**, 043815 (2011).
[32] Y. O. Dudin, L. Li, and A. Kuzmich, Phys. Rev. A **87**, 031801(R) (2013).
[33] See the Supplemental Material at http://link.aps.org/supplemental/10.1103/PhysRevLett.125.013601 for theory, numerical simulation, and experimental details, which includes Refs. [34–42]
[34] S. Walter, A. Nunnenkamp, and C. Bruder, Ann. Phys. (Amsterdam) **527**, 131 (2015).
[35] D. M. Goldberg and J. R. Gott, Cartographica **42**, 297 (2007).
[36] M. Fleischhauer and M. D. Lukin, Phys. Rev. Lett. **84**, 5094 (2000).
[37] M. D. Lukin, Rev. Mod. Phys. **75**, 457 (2003).
[38] M. Fleischhauer, A. Imamoglu, and J. P. Marangos, Rev. Mod. Phys. **77**, 633 (2005).
[39] R. Grobe, F. T. Hioe, and J. H. Eberly, Phys. Rev. Lett. **73**, 3183 (1994).
[40] D. A. Steck, Rubidium 87 D line data, available online at http://steck.us/alkalidata.
[41] C. N. Cohen-Tannoudji, Rev. Mod. Phys. **70**, 707 (1998).
[42] U. Schünemann, H. Engler, R. Grimm, M. Weidemüller, and M. Zielonkowski, Rev. Sci. Instrum. **70**, 242 (1999).
[43] R. Gilmore, C. M. Bowden, and L. M. Narducci, Phys. Rev. A **12**, 1019 (1975).
[44] K. Husimi, Proc. Phys. Math. Soc. Jpn. **22**, 264 (1940).
[45] Y. Lee Loh and M. Kim, Am. J. Phys. **83**, 30 (2015).
[46] J. M. Radcliffe, J. Phys. A **4**, 313 (1971).
[47] A. W. Laskar, N. Singh, A. Mukherjee, and S. Ghosh, New J. Phys. **18**, 053022 (2016).
[48] R. H. Dicke, Phys. Rev. **93**, 99 (1954).